Materials Research Express

PAPER

Particle size influence on material properties of $BaTiO_3$ ceramics fabricated using freeze-form extrusion 3D printing

To cite this article: Anabel Renteria *et al* 2019 *Mater. Res. Express* **6** 115211

Materials Research Express

PAPER

Particle size influence on material properties of $BaTiO_3$ ceramics fabricated using freeze-form extrusion 3D printing

RECEIVED
18 July 2019

REVISED
25 September 2019

ACCEPTED FOR PUBLICATION
2 October 2019

PUBLISHED
16 October 2019

Anabel Renteria[1], Jorge A Diaz[1], Baitong He[2], Ivan A Renteria-Marquez[3], Luis A Chavez[1], Jaime E Regis[1], Yingtao Liu[4], David Espalin[1], Tzu-Liang (Bill) Tseng[3] and Yirong Lin[1]

[1] Department of Mechanical Engineering, The University of Texas at El Paso, El Paso 79968, United States of America
[2] Department of Physics, Shantou University, Shantou 515000, People's Republic of China
[3] Department of Industrial, Manufacturing, and Systems Engineering, The University of Texas at El Paso, El Paso 79968, United States of America
[4] Department of Aerospace and Mechanical Engineering, The University of Oklahoma, Norman, OK, 73019, United States of America

E-mail: arenteriamarquez@miners.utep.edu

Keywords: barium titanate, freeze-form extrusion, additive manufacturing, piezoelectric, dielectric

Abstract

Barium titanate ($BaTiO_3$; BTO) is a well-known lead-free piezoelectric material commonly used for sensors and actuators applications. There are several traditional methods to fabricate bulk BTO ceramics; however, most of those methods have restrictions regarding being able to produce a functional and complex shape for specific application needs. Recently, additive manufacturing techniques such as binder jetting have enabled the fabrication of complex designs of piezoelectric ceramics. However, the density achieved is relatively low thus narrowing their applications. This paper presents the fabrication of high-density $BaTiO_3$ ceramics using Freeze-form Extrusion Fabrication (FEF). The influence on material properties for different ceramic particle size was assessed. It was found that parts printed using finer $BaTiO_3$ particle sizes achieved better results in terms of density, piezoelectric, and dielectric properties. For this study, the 100 nm $BaTiO_3$ samples achieved 85.24% density, a high piezoelectric property of 204.61pC/N and dielectric permittivity of 2551. These results demonstrated the feasibility of using FEF additive manufacturing to fabricate high-quality functional ceramics with designed geometry in a mold-free fashion.

1. Introduction

Ferroelectric ceramics with piezoelectric properties are widely used in industry for sensors and actuators applications [1–4]. Lead oxide ceramics, such as lead zirconate titanate or PZT is widely used for electronic applications due to its good piezoelectric coefficient [4–6]. However, lead oxide is a toxic material that increase environmental pollution [5, 6]. Therefore, the fabrication of lead-free ceramics with excellent piezoelectric properties is an area of research interest. Barium titanate ($BaTiO_3$; BTO) is one of the most used lead-free ceramics due to its good piezoelectric (d_{33}: $\sim$ 190 pC/N) properties for building sensors, capacitors, and energy storage devices [6]. Nonetheless, the piezoelectric theoretical value of $BaTiO_3$ is relatively low in comparison with the theoretical value of PZT (d_{33}: $\sim$ 500–600 pC/N) [7]. Many studies have been focus on improving the piezoelectric coefficient of $BaTiO_3$. Huan *et al* fabricated $BaTiO_3$/PVB disks by traditional manufacturing to analyze the grain size influence on the piezoelectric property by evaluating different settings for a two-step sintering process. Results demonstrate that two-step sintering achieves a grain size of 1 μm and a maximum piezoelectric coefficient of 519 pC/N [8]. Zhu *et al* fabricated $BiFeO_3$-$BaTiO_3$ disks to evaluate the sintering effect on the piezoelectric property and grain growth, obtaining a high value of 208 pC/N [9]. However, the capacity to fabricate different designs by traditional manufacturing as described in [8, 9] were limited to the mold's shape and size.

Additive manufacturing enables the fabrication of complex designs of ceramics at a relatively low cost [10]. Different additive manufacturing techniques, such as material extrusion, binder jetting, direct energy deposition

and stereolithography have been reported in the fabrication of ceramics [11, 12]. Many studies have been focusing on the fabrication of different geometries of piezoelectric ceramics using 3D printing techniques. Kim *et al* fabricated $BaTiO_3$/PVDF nanocomposites through fused deposition modeling technique achieving a piezoelectric response after thermal poling of d_{31} of 21×10^{-3} pC/N [13]. Gaytan *et al* fabricated $BaTiO_3$ samples using binder jetting 3D printing technique achieving a theoretical density of 65.2% and a piezoelectric coefficient of 74.1 pC/N [14]. Although different additive manufacturing techniques were used to fabricate piezoelectric ceramics with complex designs, the density and mechanical properties were relatively low compared with the theoretical values.

Freeze-form Extrusion Fabrication (FEF) is a free-forming technique of Additive Manufacturing. FEF consists in the extrusion of an aqueous paste through a nozzle, which is deposited in a layer-by-layer fashion at low temperature (i.e., freezing point of the paste) [15]. This paste extrusion technique has some advantages compared with other material extrusion methods. FEF is an inexpensive and fast printing method used for rapid prototyping process technology [16]. FEF also enables the fabrication of high-density ceramics with good shape retention and mechanical properties [17]. Huang *et al* fabricated aluminum oxide (Al_2O_3) ceramics using freeze-form extrusion, resulting in high-density ceramics with an average of 90% of the theoretical value [18]. Li *et al* fabricated complex structures of Al_2O_3 using Ceramic On Demand Extrusion (CODE) technique, achieving good dimensional accuracy after sintering (15%–19% shrinkage) and high-density ceramics with 97.5% theoretical value [19]. Although this technique is widely used due to the return of good material property, there is still little work reported on the feasibility of printing ferroelectric ceramics.

This paper describes a method to fabricate high-density bulk $BaTiO_3$ piezoelectric ceramics suspensions using polyvinyl alcohol (PVA) in deionized water solution. PVA is a water-soluble and biodegradable polymer that presents an elastic structure at low temperatures [20, 21]. This elastic structure facilitates the extrusion process and improves shape retention of desired geometry due to shear-thinning behavior [22]. Furthermore, the evaluation of different particle size in the ceramic suspensions needs to be evaluated. Literature suggests that grain size plays an important role on density and material properties of ceramics [23]. Therefore, formulation of the suspension and powder particle size have an essential role to fabricate high-density ceramics. Here, three different $BaTiO_3$ particle sizes were evaluated using the same binder content. Aiming to determinate the optimal results in terms of materials properties with respect to the theoretical values of pure $BaTiO_3$. This study proves the feasibility of using FEF technique in the fabrication of excellent mate applications.

2. Experimental details

2.1. Materials, synthesis and fabrication

Three different particle size of $BaTiO_3$ powder (100 nm, 300 nm, and 500 nm; Inframat, Manchester, CT) were selected to evaluate the effect of the piezoelectric response of ceramics. Polyvinyl alcohol (PVA) powder (Mw~89,000–98,000; Sigma Aldrich, St. Louis, MO) was used as a binder for the paste fabrication.

A PVA aqueous solution was prepared by dissolving 13 wt% PVA powder in deionized water under a heavy stirring of 500 rpm. The PVA in water solution was let to dwell and stirred for 20 min to ensure homogenization. Then, the solution was placed on a hot plate at 90 °C for 20 min. The heating process allowed a complete dissolution of PVA powder in aqueous solution. After that, 70 wt% $BaTiO_3$ powder (e.g., 100 nm, 300 nm, 500 nm) was added gram by gram to the PVA solution and mixed by hand using a glass rod until a homogenous paste was obtained. The $BaTiO_3$ content in the slurry was determined by its capability to flow through the 1 mm nozzle without experience any clogging. The paste was gently deposited into a syringe tube (60 ml; Soft-Ject, Virginia Beach, VA). Figure 1 illustrates the paste preparation process. The final paste composition represents 28.5 vol% of solid loadings, 7.4 vol% of binder and 64.1 vol% of solvent. This is in good agreement with literature as researches reported solid loading contents of up to 30 vol% of $BaTiO_3$ for slurry fabrication [21]. After the paste preparation, the loaded syringe was placed in the fridge at 5 °C for 2 h. The paste was aged at low temperature to activate the elastic structure of PVA [22], which helped to achieve a constant material flow rate due to an increase in the viscoelastic response [23]. Aging also contributes to an increase in the storage modulus (G'), which facilitated the layer-by-layer stacking of material [23]. The extrusion of paste in a cold environment improved shape retention of green bodies, and facilitated the stack of material to a higher number of layers and compiled different geometries.

2.2. Printing process

Ceramic samples were printed in a modified *Printrbot Simple Metal* 3D printing machine. Figure 2(a) describes the 3D printing structure, which consists of a piston that applies force over a plunger to extrude the material through a nozzle. A cylindrical geometry was selected to evaluate the particle size influence of $BaTiO_3$. The dimensions of the sample were set to 25 mm for the outer diameter, 10 mm for the inner diameter and 13 mm

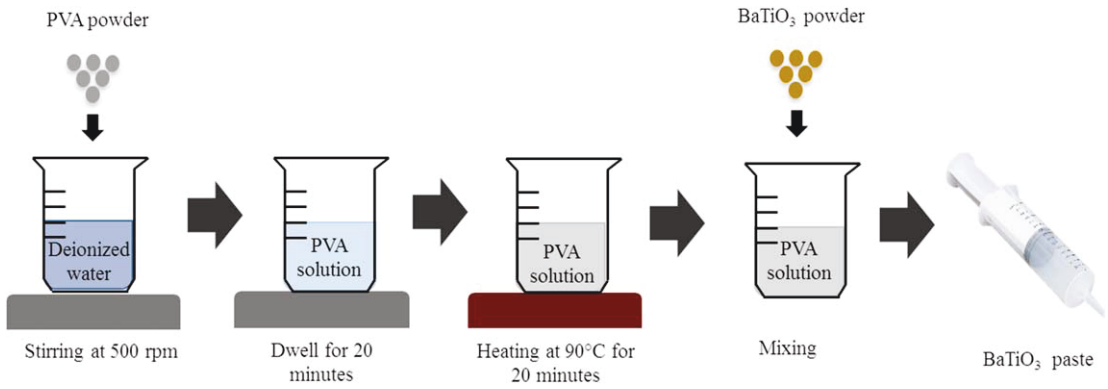

Figure 1. Schematic procedure for BTO/PVA aqueous paste.

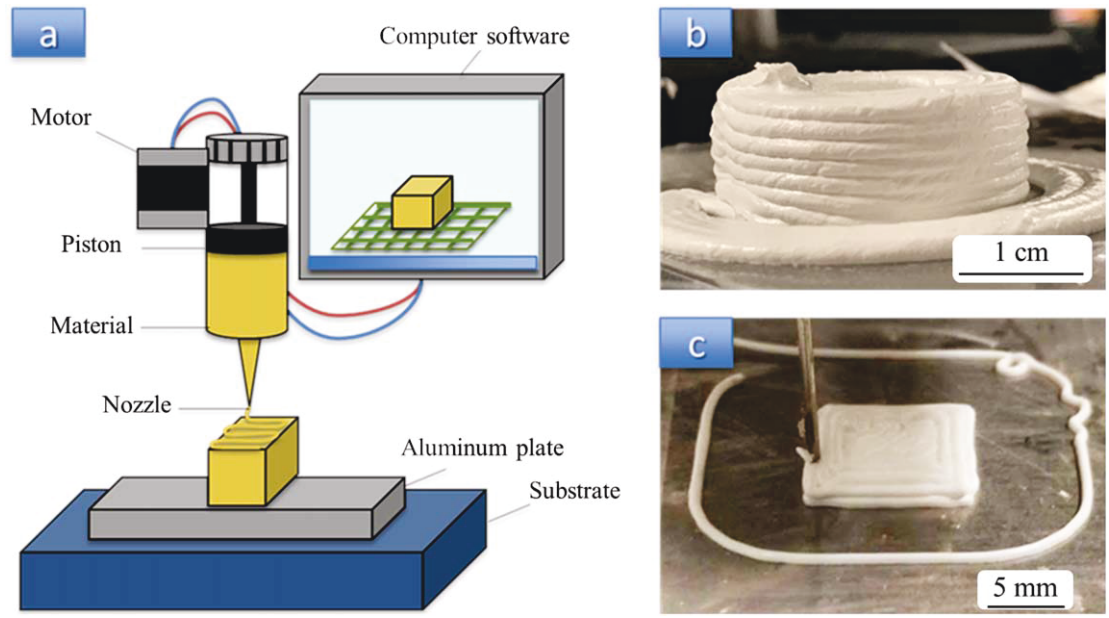

Figure 2. (a) Structure of 3D printing machine used for paste extrusion (b) 3D printed cylinder structure (c) 3D printing process of a square structure.

height. The ceramic suspensions were deposited onto an aluminum froze plate at −40 °C, which was placed into the 3D printer substrate. The plate was covered with a thin film to facilitate the detach of green bodies after the printing process. Figures 2(b) and (c) shows a cylinder and a square 3D printed structures respectively using FEF technique. Samples were printed using a nozzle diameter of 1 mm, with a speed of 10 mm s^{-1}, layer height of 0.6 mm and infill set to 80%.

After printing, the aluminum plate was removed from the printer bed and placed in the freezer at –60 °C (Thermo Scientific TSU^{TM} Series −86 °C Upright Ultra-Low) for 2 h to dry some of the water by sublimation to retain printed structural shape. Samples were detached from the aluminum plate, and it was found that the samples accumulated water on the bottom surface. To obtain homogeneous dried green bodies, the samples were turned upside down and placed back to the freezer for 30 min. A freeze-dried process contributes to shape retention and avoid warping of green bodies [24]. After that, the samples were placed in the oven (Lab companion OF-01E) at 40 °C for 24 h to remove any remaining water from the green body. Drying process at low temperatures for extended periods helps to avoid the generation of micro cracks in the green bodies [25, 26].

2.2.1. Post-processing

To increase the density of the green bodies without causing any defect, such as external micro cracks, the sintering cycle of the samples were scheduled as follows. First, debinding to allow the PVA burnout followed by sintering of the sample to enable the grain size growth. All the samples were debinded at 600 °C for one hour and 5 °C min^{-1} ramp, then sintered at 1250 °C for two hours using 5 °C min^{-1} ramp. Lastly, samples were cool

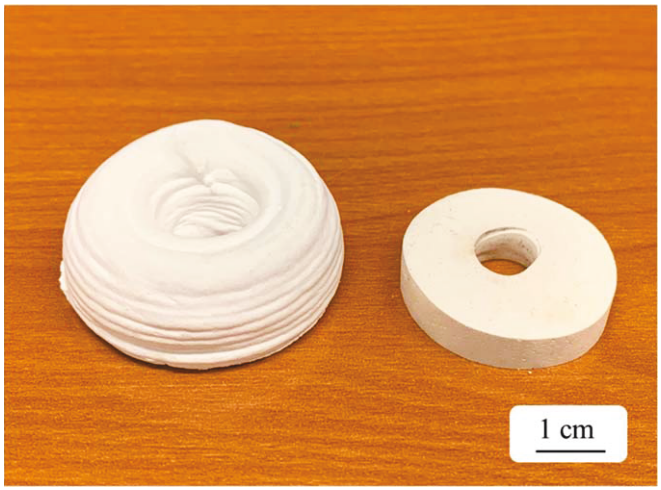

Figure 3. $BaTiO_3$ ceramic samples, green body (left) and sintered and polished (right).

down at a 5 °C min^{-1} ramp to room temperature. After sintering, the samples were polished using 240-grit sandpaper to facilitate the dipole alignment poling process. Figure 3 shows two $BaTiO_3$ ceramic samples, a green body after drying (left) and a sintered and polish sample (right). Conductive silver paint was applied on top and bottom surfaces and dried at 200 °C for 30 min. Thermal poling was performed under an electrical field of 5.4 KV cm^{-1} and submerged in silicon oil at 90 °C for two hours [27].

2.2.2. Material characterization

Rheological properties of each $BaTiO_3$-PVA suspension was measured in a DHR-2 rheometer (TA Instruments, New Castle, DE) with a parallel plate geometry. The gap between the plates was set to 1.2 mm, and the test was performed at 25 °C. The apparent density of the samples was measured by using the Archimedes' method. Then, compared with the theoretical value of pure $BaTiO_3$ of 6.02 g cm^{-3} [28]. The piezoelectric coefficient was calculated using a d_{33} meter (APC YE2730A). Dielectric permittivity was calculated using an LCR meter (1920 Precision, IET lab). The grain morphology characterization for different 3D printed $BaTiO_3$ ceramics was observed by scanning electron microscope (SEM, TM-1000 Hitachi). Crystal structured was analyzed by x-ray diffraction (XRD) using CuKα radiation on a D8 discover diffractometer (Bruker).

3. Results and discussion

The slurry composition plays a critical role during the printing process, especially for shape retention and printability [29]. The rheological properties of the slurry are highly influenced by the solid loadings content. Low solid loading contents produces a low viscous suspension, with a Newtonian behavior [30], which makes it unsuitable for printing. Low viscous slurries will tend to collapse as the number of layers of material increase [22]. In another hand, high solid loadings contents produces high viscous slurries with a high shear-thinning behavior [30]. High viscous suspensions restrict particle mobility, [30] increasing the probabilities of clogging during printing. Moreover, the shear stress over the walls of the nozzle will rise and higher yield strength will be required [22].

Figure 4 shows the results of viscosity as a function of shear rate for different $BaTiO_3$-PVA suspensions varying powder particle size. A high influence on the rheological results was observed for different ink compositions. The ceramics suspensions index for a shear thinning behavior [23, 31] since a reduction in viscosity was observed when increasing the applied shear rate. The shear thinning behavior can be attributed to the PVA content in the suspensions. PVA behaves as a non-Newtonian fluid and exhibits different viscoelastic properties depending on the concentration and molecular weight [31]. Additionally, a higher initial viscosity at low shear rates was observed for finer particles, which decreases at high shear rates. The stress profile under different shear rates is shown in figure 5. It was found that a higher yield strength was required for finer particle size to generate the initial flow through the nozzle. Once the flow is initialized, the yield strength required for printing stabilizes and remains in a constant range. The change in the yield strength to a constant phase can be attributed to a laminar flow behavior of the suspensions [29], which facilitate the deposition of material onto the substrate. Furthermore, literature indicates that particle size plays an important role in the rheology of the suspensions. Finer sizes increases the contact between the particles dispersed in the suspension increasing the

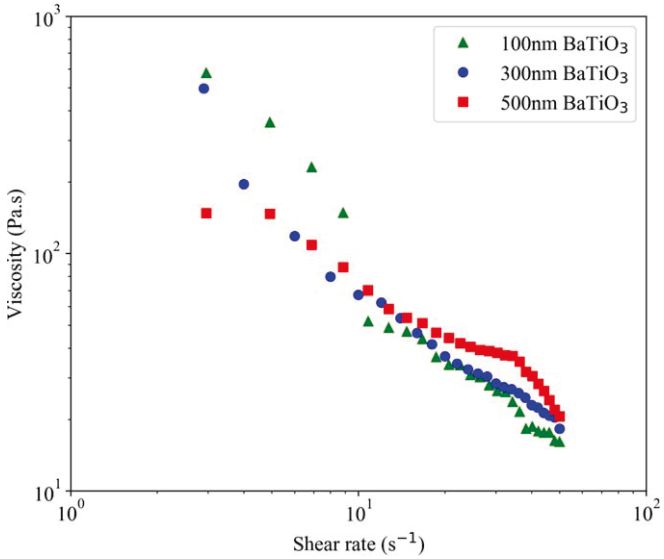

Figure 4. Evolution of viscosity as a function of shear rate for $BaTiO_3$-PVA suspensions with 100 nm, 300 nm and 500 nm particle size.

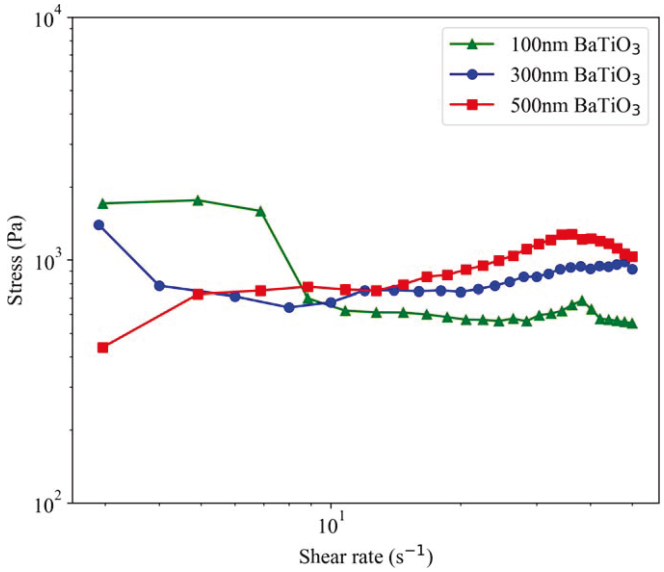

Figure 5. Stress behavior as a function of shear rate for $BaTiO_3$-PVA suspensions with 100 nm, 300 nm, and 500 nm particle size.

viscosity [32]. The increase in viscosity can be attributed to liquid trapped inside aggregates of powder within the paste [33]. Moreover, finer particles are affected by Van der Walls forces, producing agglomerations in the slurries, which limits the matrix fluid [30]. In addition, the yield strength required to initialize the flow will increase, affecting the printing process.

3.1. SEM and XRD analysis

The SEMs from the top surface and cross-section were observed to gain information about the microstructure and the porosity of the samples for different powder particles. The sintered samples were fractured to observe the microstructure from the cross-sectional area. Figure 6(A)) presents a sample that was fabricated using 100 nm particle size. The average grain grow of $\phi \simeq 1.18$ μm was observed. Samples using 300 nm and 500 nm particle size are illustrated in figures 6(B)–(C)) respectively. An average grain size of $\phi \simeq 0.871$ μm for the 300 nm and $\phi \simeq 0.757$ μm for the 500 nm were observed. It was found that the average grain size after sintering decrease when increasing the powder particle size. Literature suggests that the final grain size after sintering is highly dependent of sintering temperature, exposure time and powder particle size [34]. Furthermore, reducing the powder particle size results in a higher curvature of the ceramic powder, meaning that a lower change in energy is

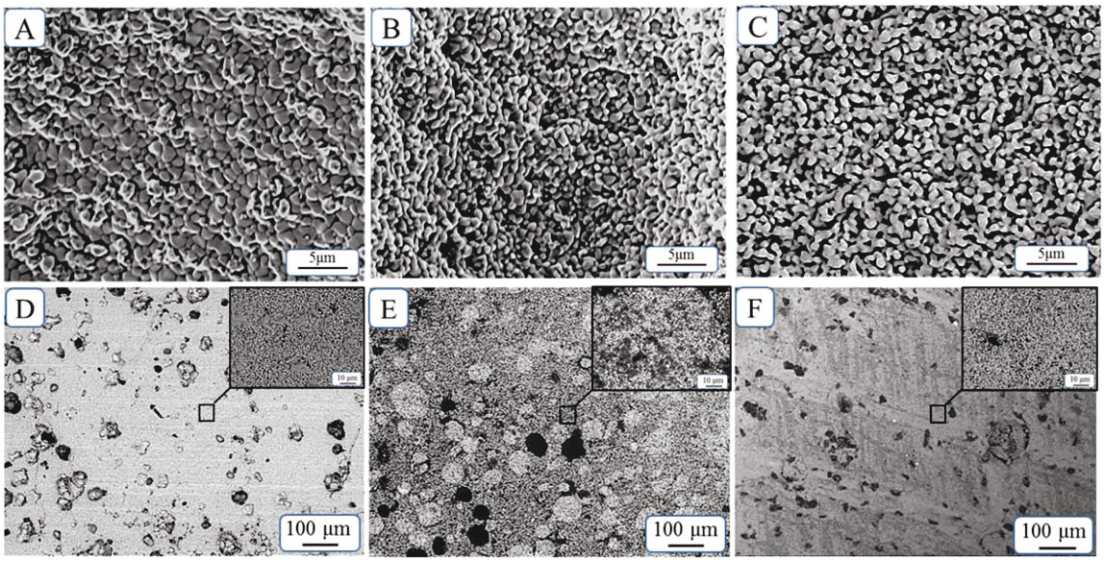

Figure 6. $BaTiO_3$ samples after sintering at 1250 °C. Cross-section for (A) 100 nm sample (B) 300 nm sample and (C) 500 nm sample. Top surface and surface microstructure for (D) 100 nm sample (E) 300 nm sample and (F) 500 nm samples.

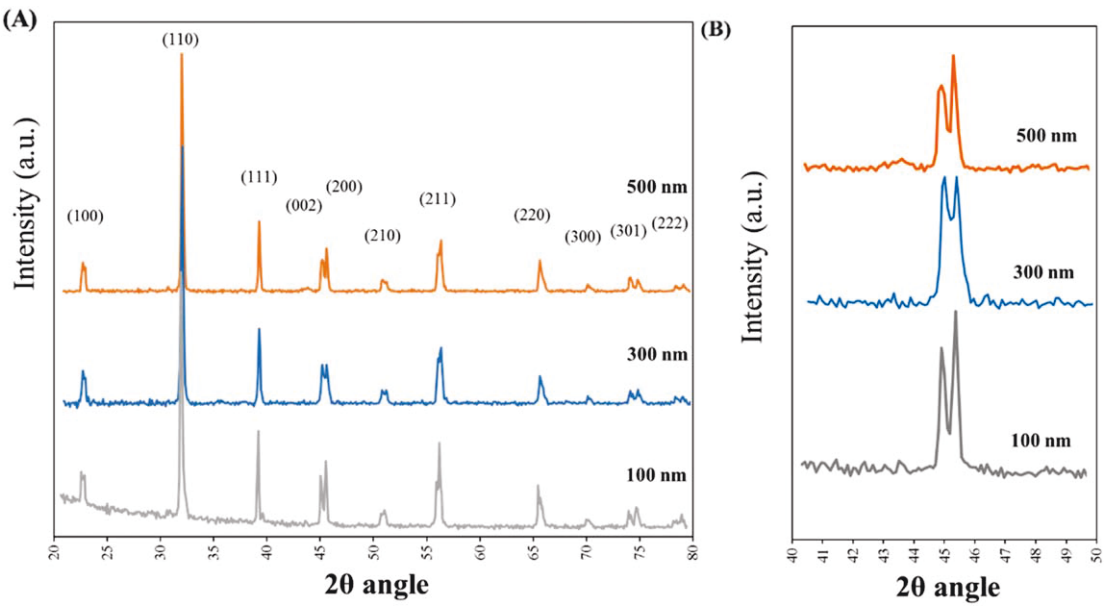

Figure 7. (A) XRD for $BaTiO_3$ for 100 nm, 300 nm and 500 nm powder particle size in range 2θ: from 20° to 80°. (B) XRD at peaks (002) and (200) in a range 2θ: from 40° to 50°.

required during sintering [35]. Figures 6(D):(F) show the top surface for the 100 nm, 300 nm and 500 nm respectively. A reduction on the number of pores and pores sizes were observed when decreasing the powder particle size. The 100 nm sample showed a few voids ranging from 50 μm to 1 μm. However, the voids are not very deep as some grains can be observed inside the void. The 300 nm sample presents a more porous surface as voids of around 70 μm were observed. The 500 nm sample showed voids in the range of 25 μm to 5 μm at higher magnifications. However, the number of voids around the top surface were more than the 100 nm and 300 nm samples. The results obtained from the top surface complements the grain growth and porosity observed from the cross-sectional area. The reduction of pores for the 100 nm sample can be attributed to a higher rate of densification and a more uniform grain boundary.

The XRD for different $BaTiO_3$ particle size are shown in figure 7. The samples were evaluated in a range 2θ: from 20° to 80° at room temperature after poling process. The peaks observed in figure 7(A) index for tetragonal crystal structure [36, 37]. The peaks splitting observed around at 2θ: 45°, 51°, 56° and 75° indicates a phase transformation from cubic structure. Furthermore, the peak splitting observed at (002) and (200) confirms the

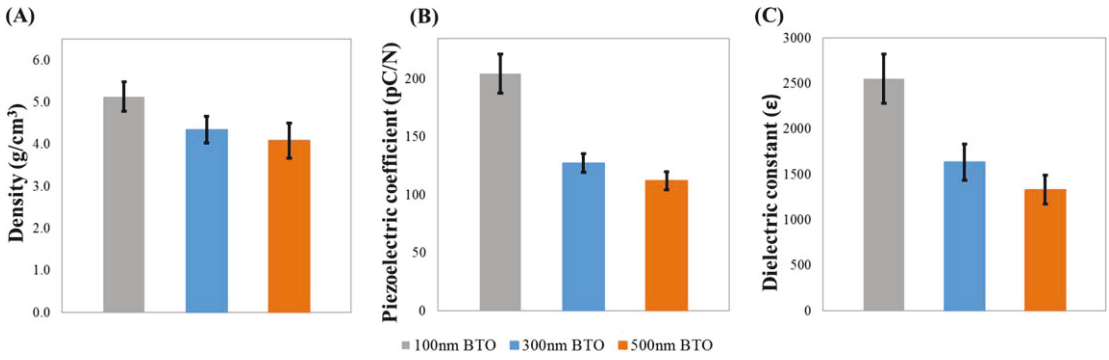

Figure 8. Average result of density, piezoelectric coefficient and dielectric constant.

tetragonality phase of the samples, as shown in figure 7(B). Phase transformation on $BaTiO_3$ can be observed for heat treatments above 1000 °C [38]. Moreover, $BaTiO_3$ remains in the tetragonal crystal structure at room temperature, however the curie temperature at which it will transform to cubic is 120 °C [39]. The 100 nm sample showed a higher peak splitting intensity, which indicates a higher degree of crystallinity. These results are in good agreement with literature according to the following points. Several studies indicate that ferroelectric domain is influence by the size of the crystals [40], which can be controlled by the heat treatment temperature [39–42]. The $BaTiO_3$ samples were exposed to the same treatment temperature of 1250 °C for the same period of time. The difference on degrees of crystallinity are attributed to the final grain growth obtained during the sintering process.

3.2. Material properties

Figure 8(A) shows the density results obtained for different particle size after sintering process. The relative densities for the 100 nm, 300 nm and 500 nm were 5.13 ± .35 g cm^{-3}, 4.35 ± .32 g cm^{-3} and 4.09 ± .42 g cm^{-3} respectively; which correspond to 85.24% ± 5.74%, 72.19% ± 5.27% and 67.94% ± 6.91% of the theoretical value for pure $BaTiO_3$. It was found that the relative density after sintering increased when reducing the powder particle size. This is in good agreement with the grain-growth observed from the SEMs microstructure. Coarse powder particles showed a lower increase in the final grain-growth, which increase the number of voids on the samples. Additionally a higher level of porosity can led to lower material properties. The piezoelectric coefficient results are presented in figure 8(B). A positive increment on the d_{33} was observed for finer powder particles. The piezoelectric coefficient (d_{33}) were 204.61 ± 16.87 pC/N, 127.63 ± 8.19 pC/N and 112.2 ± 7.99 pC/N for the 100 nm, 300 nm and 500 nm respectively; which correspond to 107.12% ± 8.83, 66.82% ± 4.29 and 58.74% ± 4.18 of the theoretical value of 191 pC/N [28]. The increment on the piezoelectric coefficient can be attributed to the higher grain growth at the micron level when using finer particles [28, 40, 41]. Different studies suggest that there is a strong dependency in the grain size and the piezoelectric properties [28]. Furthermore, $BaTiO_3$ crystalline structure is influenced by the domain walls width, which contributes to the piezoelectric response. Grain size in the micron level decrease the 90° domain width, producing a smaller domain walls [8]. The decrease in the domain walls facilitate its rotation, which increase the sensibility to an external stress or electrical signal [8, 42]. Figure 8(C) shows the dielectric permittivity (ε) results, the measurements were performed at 25 °C with a frequency of 1 kHz. The dielectric permittivity obtained for the 100 nm, 300 nm, and 500 nm, which were 2250 ± 270, 1636.34 ± 199.7 and 1333.07 ± 157 respectively. These values correspond to 115.38% ± 13.84, 83.89% ± 10.24 and 68.35% ± 8.05 of the theoretical value of $BaTiO_3$ of 1950 at 90 °C [40]. Different studies suggest that the dielectric constant increase when the grain growth is at the micron level [43–45]. Additionally, a uniform grain-size distribution is required to achieve a higher permittivity [46, 47]. Furthermore, residuals of binder content of the sample may influence the dielectric permittivity results. Literature suggest that impurities such as carbon residues may be encapsulated inside the sample increasing the permittivity [48, 49]. Finer particles reached higher density with a significant lower number of voids, reducing the space in the grain boundaries, preventing the escape of carbon from the sample during sintering increasing the permittivity.

The results obtained for density and material properties are comparable with previous studies that report the fabrication of piezoelectric ceramics using Additive Manufacturing. For robocasting, [4] reported a density of 65.3%, a piezoelectric coefficient of 200 pC/N and a dielectric permittivity of 4730 at 1 KHz for $BaTiO_3$. In the fabrication of PZT composites a piezoelectric coefficient of 300 pC/N and dielectric permittivity if 2250 at 10 KHz [50]. In another hand, for binder jetting, [14] a density of 65.2%, a piezoelectric of 74 pC/N and a dielectric permittivity of at 1 KHz for $BaTiO_3$ were reported. This study contributes with a fabrication method for $BaTiO_3$

ceramics with higher density and similar material properties as previous published works. Proving the feasibility of the slurry composition and FEF technique.

4. Conclusion

A simple method to fabricate high-density $BaTiO_3$ ceramics using freeze-form extrusion fabrication (FEF) was presented. Three different particle size of $BaTiO_3$ were investigated in terms of their influence on density, piezoelectric coefficient, and dielectric permittivity. Results showed that finer $BaTiO_3$ particles could lead to better material property due to a higher grain growth after sintering. Using 100 nm particle size, a density of $5.13 \pm .35$ g cm^{-3} can be achieved, which correspond to 85.24% $\pm$ 5.74 of the theoretical value. A high piezoelectric coefficient (d_{33}) of 204.61 $\pm$ 16.87 pC/N was obtained, corresponding to 107.12% $\pm$ 8.83 of the theoretical value of 191 pC/N. A dielectric constant of 2551.09 $\pm$ 270 at 1 KHz was obtained, representing 115.38% $\pm$ 13.84 of the theoretical of 1950. The grain size and morphology was observed through SEM, which corroborated the experimental results on density, piezoelectric and dielectric. XRD analysis confirmed the tetragonal crystal structure in the samples after sintering. These results demonstrated the feasibility of using FEF technique as an inexpensive method for rapid prototyping design of bulk piezoelectric devices such as sensors and actuators with the possibility of a high degree of customization and excellent material properties.

Acknowledgments

This research is funded by Department of Energy (DOE) under Grant No. DE-FE0027502, and DE-NA0003865.

ORCID iDs

Anabel Renteria https://orcid.org/0000-0001-9013-8115
Luis A Chavez https://orcid.org/0000-0001-5203-6708
Yingtao Liu https://orcid.org/0000-0002-6232-9704

References

[1] Nonkumwong J, Sriboriboon P, Kundhikanjana W, Srisombat L and Ananta S 2018 Ferroelectric domain evolution in gold nanoparticle-modified perovskite barium titanate ceramics by piezoresponse force microscopy *Integr. Ferroelectr.* **187** 210–8
[2] Renteria-Marquez I A, Renteria-Marquez A and Tseng B 2018 A novel contact model of piezoelectric traveling wave rotary ultrasonic motors with the finite volume method *Ultrasonics* **90** 5–17
[3] Renteria-Marquez I A and Bolborici V 2017 A dynamic model of the piezoelectric traveling wave rotary ultrasonic motor stator with the finite volume method *Ultrasonics* **77** 69–78
[4] Kim H *et al* 2018 Fabrication of bulk piezoelectric and dielectric $BaTiO_3$ ceramics using paste extrusion 3D printing technique *J. Am. Ceram. Soc.* **102** 3685-3694
[5] Maeder M D, Damjanovic D and Setter N 2004 Lead free piezoelectric materials *J. Electroceram.* **13** 385–92
[6] Shrout T R and Zhang S 2007 Lead-free piezoelectric ceramics: alternatives for PZT? *J. Electroceram.* **19** 185
[7] Liu W and Ren X 2009 Large piezoelectric effect in Pb-free ceramics *Phys. Rev. Lett.* **103** 257602
[8] Huan Y, Wang X, Fang J and Li L 2013 Grain size effects on piezoelectric properties and domain structure of $BaTiO_3$ ceramics prepared by two-step sintering *J. Am. Ceram. Soc.* **96** 3369–71
[9] Zhu L-F *et al* 2018 Enhanced piezoelectric and ferroelectric properties of $BiFeO_3$-$BaTiO_3$ lead-free ceramics by optimizing the sintering temperature and dwell time *J. Eur. Ceram. Soc.* **38** 3463–71
[10] Conner B P *et al* 2014 Making sense of 3D printing: creating a map of additive manufacturing products and services *Additive Manufacturing.* **1–4** 64–76
[11] Deckers J, Vleugels J and Kruth J-P 2014 Additive manufacturing of ceramics: a review *Journal of Ceramic Science Technology.* **5–4** 245–60
[12] Mason M S, Huang T, Landers R G, Leu M C and Hilmas G E 2009 Aqueous-based extrusion of high solids loading ceramic pastes: process modeling and control *J. Mater. Process. Technol.* **209** 2946–57
[13] Kim H, Fernando T, Li M, Lin Y and Tseng T-L B 2017 Fabrication and characterization of 3D printed $BaTiO_3$/PVDF nanocomposites *J. Compos. Mater.* **52** 197–206
[14] Gaytan S *et al* 2015 Fabrication of barium titanate by binder jetting additive manufacturing technology *Ceram. Int.* **41** 6610–9
[15] Leu M C, Deuser B K, Tang L, Landers R G, Hilmas G E and Watts J L 2012 Freeze-form extrusion fabrication of functionally graded materials *CIRP Ann.* **61** 223–6
[16] Lu X, Lee Y, Yang S, Hao Y, Evans J R and Parini C G 2010 Solvent-based paste extrusion solid freeforming *J. Eur. Ceram. Soc.* **30** 1–10
[17] Wei X, Nagarajan R S, Peng E, Xue J, Wang J and Ding J 2016 Fabrication of YBa_2 Cu_3O_{7-x} (YBCO) superconductor bulk structures by extrusion freeforming *Ceram. Int.* **42** 15836–42
[18] Huang T, Mason M S, Hilmas G E and Leu M C 2006 Freeze-form extrusion fabrication of ceramic parts *Virtual and Physical Prototyping.* **1** 93–100
[19] Li W, Ghazanfari A, Mcmillen D, Leu M C, Hilmas G E and Watts J 2017 Fabricating ceramic components with water dissolvable support structures by the Ceramic On-Demand Extrusion process *CIRP Ann.* **66** 225–8

[20] Zhou W, Nie Y M, Li S J and Liang H Y 2013 The importance of the solids loading on confirming the dielectric nanosize dependence of $BaTiO_3$ powders by slurry method *The Scientific World Journal.* **2013** 1–3
[21] Fumio U, Hiroshi Y, Kumiko N, Sachihiko N, Kenji S and Yasunori M 1990 Swelling and mechanical properties of poly(vinyl alcohol) hydrogels *Int. J. Pharm.* **58** 135–42
[22] M'Barki A, Bocquet L and Stevenson A 2017 Linking rheology and printability for dense and strong ceramics by direct ink writing *Sci. Rep.* **7** 6017
[23] Hoshina T *et al* 2018 Grain size effect on piezoelectric properties of $BaTiO_3$ ceramics *Japan. J. Appl. Phys.* **57** 1-5
[24] Travitzky N *et al* 2014 Additive manufacturing of ceramic-based materials *Adv. Eng. Mater.* **16** 729–54
[25] Misra R 2002 Controlled drying to enhance properties of technical ceramics *Chem. Eng. J.* **86** 111–6
[26] Amza C, Zapciu A and Popescu D 2017 Paste extruder—hardware add-on for desktop 3D Printers *Technologies.* **5** 50
[27] Novak N, Pirc R and Kutnjak Z 2014 Effect of electric field on ferroelectric phase transition in $BaTiO_3$ ferroelectric *Ferroelectrics* **469** 61–6
[28] Mason W P and Matthias B T 1948 Theoretical model for explaining the ferroelectric effect in barium titanate *Phys. Rev.* **74** 1622–36
[29] Lewis J A 2006 Direct ink writing of 3D functional materials *Adv. Funct. Mater.* **16** 2193–204
[30] Kaully T, Siegmann A and Shacham D 2007 Rheology of highly filled natural $CaCO_3$ composites. II. Effects of solid loading and particle size distribution on rotational rheometry *Journal of Polymer Composites.* **28** 524–33
[31] Gao H-W, Yang R-J, He J-Y and Yang L 2009 Rheological behaviors of PVA/H_2O solutions of high-polymer concentration *J. Appl. Polym. Sci.* **116** 1459–66
[32] Do T-A, Hargreaves J, Wolf B, Hort J and Mitchell J 2007 Impact of particle size distribution on rheological and textural properties of chocolate models with reduced fat content *J. Food Sci.* **72** E541–E552
[33] Demerlis C and Schoneker D 2003 Review of the oral toxicity of polyvinyl alcohol (PVA) *Food Chem. Toxicol.* **41** 319–26
[34] Yoon B-K, Lee B-A and Kang S-J L 2005 Growth behavior of rounded (Ti,W)C and faceted WC grains in a Co matrix during liquid phase sintering *Acta Mater.* **53** 4677–85
[35] Ting J-M and Lin R Y 1994 Effect of particle-size distribution on sintering *J. Mater. Sci.* **29** 1867–72
[36] Cullity B D 2015 *Elements of X-ray Diffraction* (Utgivningsort okänd: Scholars Choice)
[37] Wei Y *et al* 2014 Dielectric and ferroelectric properties of $BaTiO_3$ nanofibers prepared via electrospinning *Journal of Materials Science & Technology.* **30** 743–7
[38] Gebwein H, Hanemann T, Haubelt J and Schumacher B 2008 Influence of the crystallite size of $BaTiO_3$ on the dielectric properties of polyester reactive resin composite materials *Tech. Connect Briefs.* **1** 385–8
[39] Evans H T 1961 An x-ray diffraction study of tetragonal barium titanate *Acta Crystallographica.* **14** 1019–26
[40] Hsiang H-I, Lin K-Y, Yen F-S and Hwang C-Y 2001 Effects of particle size of $BaTiO_3$ powder on the dielectric properties of $BaTiO_3$/polyvinylidene fluoride composites *Journal of Materials Science* **36** 3809–15
[41] Elqudsy M A, Widodo R D, Rusiyanto R and Sumbodo W 2017 The particle and crystallite size analysis of $BaTiO_3$ produced by conventional solid-state reaction process. *AIP Conf Proc* 10.1063/1.4976876
[42] Huan Y, Wang X, Fang J and Li L 2014 Grain size effects on piezoelectric and ferroelectric properties of $BaTiO_3$ ceramics *J. Eur. Ceram. Soc.* **34** 1445–8
[43] Renteria A *et al* 2019 Optimization of 3D printing parameters for $BaTiO_3$ piezoelectric ceramics through design of experiments *Mater. Res. Express* **6** 085706
[44] Bjørk R, Tikare V, Frandsen H L and Pryds N 2012 The effect of particle size distributions on the microstructural evolution during sintering *J. Am. Ceram. Soc.* **96** 103–10
[45] Yong-An H *et al* 2018 Grain size effect on dielectric, piezoelectric and ferroelectric property of $BaTiO_3$ ceramics with fine grains *Journal of Inorganic Materials.* **33** 767
[46] Luan W, Gao L and Guo J 1999 Size effect on dielectric properties of fine-grained $BaTiO_3$ ceramics *Ceram. Int.* **25** 727–9
[47] Zheng P, Zhang J, Tan Y and Wang C 2012 Grain-size effects on dielectric and piezoelectric properties of poled $BaTiO_3$ ceramics *Acta Mater.* **60** 5022–30
[48] Frey M H and Payne D A 1996 Grain-size effect on structure and phase transformations for barium titanate *Phys. Rev.* B **54** 3158–68
[49] Robinson S K and Paul M R 2001 Debinding and sintering solutions for metals and ceramics *Met. Powder Rep.* **56** 24–34
[50] Yi C-H, Lin C-H, Wang Y-H, Cheng S-Y and Chang H-Y 2012 Fabrication and characterization of flexiblE PZT fiber and composite *Ferroelectrics* **434** 91–9